

Multi-Band Frequency Selective Surface with Double-Square-Loop Patch Elements

Te-Kao Wu

Jet Propulsion Laboratory
California Institute of Technology
Pasadena, California 91109

Abstract

Design, analysis and experimental verifications are presented for a multi-band frequency selective surface (IRS) with perfectly conducting double-square-loop (DSL) patch elements. A single screen double-square-loop element FSS is demonstrated for (1) a tri-band system that reflects the X-band signal while transmitting the S- and Ku-band signals, (2) a low-pass (or Ka-add-on) FSS that **reflects** the Ka-band signal **while** passing the S-, X-, and Ku-band signals, and (3) a four-band FSS which reflects the X- and **Ka-** band signals while passing the S- and Ku-band signals for the NASA Cassini Project. In addition, a double screen FSS consisting of a low-pass and a **tri-band** FSS is presented for the Cassini four-band application. The good agreement obtained between the measured and the computed results verified the single and double screen FSS approaches for the **Cassini** Project.

I. Introduction

Frequency selective surfaces (FSS) have often been considered for reflector antenna applications [1-8]. Typically, an FSS is employed for the sub reflector and the different frequency feeds are optimized independently and placed at the real and virtual foci of the subreflector. Hence, only a single main reflector is required for the multi-frequency operation. For example, the FSS on the high gain antenna (HGA) of the Voyager spacecraft was designed to diplex S and X bands [1]. In that application the S-band feed is placed at the prime focus of the main reflector, and the X-band feed is placed at the Cassegrain focal point. Note that only one main reflector is required for this two band operation. Thus, tremendous reductions in mass, volume and, most important, the cost of the antenna system are achieved with the FSS subreflector.

Recently, the NASA Cassini Project [5] required the use of multiple microwave frequencies at S-, X-, Ku- and Ka-band for science investigations and data communication links. A single HGA with an FSS subreflector, as illustrated in Figure 1, was proposed. This arrangement allows a Cassegrain configuration at X (7.2 and 8.4 GHz) and Ka (32 and 34.5 GHz) bands and a prime focus configuration at S (2.3 GHz) and Ku (13.8 GHz) bands [5-8]. Circular polarizations are required for all frequency bands except the Ku-band.

In the past, the cross-dipole patch element FSS was used for the subreflector design in the reflector antennas of Voyager [1] for reflecting the X-band waves and passing the S-band waves, and the Tracking and Data Relay Satellite System (TDRSS) for diplexing the S- and Ku-band waves [2]. The characteristics of the cross-dipole element FSS change drastically as the incident angle is steered from normal to 40°. Thus a large band separation is required to minimize the RF losses for these dual band applications. This is evidenced by the reflection and transmission band ratio (f_r/f_t) being 7:1 for a single screen FSS [2] or 4:1 for a double screen FSS [1] with cross-dipole patch elements. Much closer band spacings

and a stable bandwidth insensitive to the incident angle variation are available from dipoles sandwiched between dielectrics about $\lambda/2$ thick [9]. However, if a lighter weight structure or the circular polarization is required then thin dielectrics supported by low-mass material must be used, and other elements have to be sought.

FSSS with double square loop (DSL) and double ring patch elements have been designed for frequency band ratios (f_2/f_1) from 1.5 to 2 [3-8, 10-11]. Their resonant frequencies are fairly stable with respect to changes in the incident angle and polarizations. In addition, the grid geometry is symmetrical in the x and y directions. This implies that it is also good for circular polarizations. Hence, the DSL and double ring elements are considered for the Cassini FSS design to achieve (1) the multiplexing of four frequency bands, (2) smaller frequency-band separations (f_2/f_1 , less than 1.7), and (3) less sensitivity to the incident angle variation and polarizations. Since the double ring element FSS was discussed in [7,8], this paper will concentrate on the DSL element FSS.

To meet the Cassini antenna subsystem's RF requirements, two design approaches as shown in Figure 2, are proposed. In addition, the FSS screen was bonded on to a Kevlar honeycomb panel to meet the mechanical and thermal environmental requirements. The first approach, implementing the two-screen design, uses two FSS grids. The front FSS grid is called the **Ka-add-on** FSS. It reflects Ka-band waves but passes S-, X- and Ku- band waves. The back FSS grid is called the 3-frequency FSS. It reflects X-band waves but passes S- and Ku-band waves. The resultant FSS reflects both X- and Ka-band waves but passes both S and Ku band waves. The second approach, implementing the single screen design, uses only a single FSS grid to reflect the X- and **Ka-band** waves and to pass the S- and **Ku-** band waves. In the following sections, the analysis, design and performance of a multi-band FSS with DSL elements are demonstrated.

II. Analysis of a Single Screen DSL Element FSS

For a DSL element FSS etched on an electrically thin dielectric substrate, as illustrated in Figure 3, its transmission performance can be accurately analyzed using the Equivalent Circuit Model (ECM) [10-12]. However, in space applications, the FSS grids are required to be **imbedded** between two dielectrics and then **supported** by a **Kevlar** honeycomb sandwich structure [1-8], as illustrated in Figure 2. These dielectric materials are all space qualified materials, so the resultant FSS flight hardware can keep its physical integrity and sustain the mechanical loads in the launch and space environments. When the dielectrics are added to the free standing FSS grids, the FSS characteristics are changed significantly. This is because the dielectric materials tend to reduce and to stabilize the incident angle dependence of the FSS's resonant frequency [4,9] in the rejection band. In addition, the RF transmission loss in the pass band is increased significantly due to these lossy Kevlar materials. The ECM can not accurately model the above mentioned effects caused by the dielectrics. Thus the accurate integral equation formulation (IEF) [13-17] should be implemented for this particular application.

Previously, **two** different IEF approaches have been developed to accurately predict the effects of the dielectrics. One approach is based on entire **domain** expansion functions [13,16,17], while the other is based on **subdomain** expansion functions as described in [14,15]. **The** entire domain expansion function approach suffers from a poor convergence problem, especially for the DSL element with corners and junctions. Therefore, the **subdomain** expansion approach is selected for the design and analysis for **all** the DSL element FSS considered in this paper.

Generally, the integral equation of the FSS grid and the dielectrics is formulated by applying the **Floquet** theorem and enforcing the boundary conditions at the interfaces. The FSS's unit cell is divided into many discrete rectangular subcells [14]. **Then** the specific

1

patch element is fitted into the subcell grid. The unknown current on each conducting subcell is represented by a roof-top expansion function with an unknown coefficient. A matrix equation may be obtained by testing the integral equation with the same current expansion function. The unknown current expansion coefficients are obtained by the standard matrix inversion technique. The transmitted and reflected fields may next be evaluated from these currents.

11.1. Single Screen Tri-band FSS

The design and performance of a tri-band FSS with DSL elements can be found in [4] and are rewritten here for completeness. Figure 3 shows the design of a thin DSL element FSS on a 0.001" thick and 20" by 20" sized Kapton sheet. This DSL element FSS is designed to reflect the X band waves (8.4 GHz) and to pass the S band (2.3 GHz) as well as the Ku band (13.8 GHz) waves. This thin FSS can be analyzed both by the ECM and the IEF approaches. Figure 4 shows the calculated transmission performance obtained by both approaches as a function of the incident angle and the polarization. Excellent agreement between the ECM and the IEF is observed for the normal incidence case. This implies that, at normal incidence, this thin FSS may be considered as an electrically free standing grid, even though it is supported by a 0.001" thick Kapton sheet. Note that the resonant frequency of this DSL FSS remains near 8.4 GHz, as the incident angle is steered from 0° to 45°, for both TE and TM polarizations. This makes the DSL element FSS especially superior to the cross-dipole element FSS [1,2]. Representatively, Figure 5 shows the computed and measured transmission characteristics of the DSL element FSS with 15° TM incident plane wave. The computed results were obtained via the IEF approach [14].

As was pointed out in Section I, the FSS grids must be integrated with rigid and space qualified dielectric materials for the NASA Cassini Project. Thus another DSL element FSS was designed and fabricated as illustrated in Figure 6. Here the FSS grids were

etched on a 0.001” thick Kapton sheet and then bonded to the **Kevlar** honeycomb sandwich panel. Note these grids dimensions were designed by assuming the dielectric constant of the **Kevlar/Epoxy** skin is 2.35. Figure 7 shows the predicted and measured transmission performance of this new FSS. Note that the **resonant** frequency for this new FSS is near 8.4 GHz for incident angles from normal to $(\theta_i, \phi_i) = (45^\circ, 45^\circ)$ and for both TE and TM polarizations. The measured data agrees very well with the predicted data as shown in Figure 7 for the representative normal incidence case. This verifies the validity of the IEF design approach for the single screen **tri-band** FSS with DSL elements.

IV. Single Screen 4-Frequency FSS

In general, the DSL element FSS provides two resonances, i.e., one at a lower frequency (caused by the larger loop) and the other at a higher frequency (caused by the smaller loop). Therefore, one may be able to design a single screen DSL element FSS for the Cassini’s 4-frequency FSS. In other words, only one DSL element FSS grid is needed for reflecting the X- and **Ka-band** while passing the S- and Ku-band waves. To avoid grating lobes, the 4-frequency integrated FSS was etched on a 0.01” thick **Duroid** 6010.5 substrate. The substrate has a dielectric constant of 11 and the loss tangent is 0.0028.

The geometry and configuration of the 4-frequency FSS with a **Kevlar** honeycomb are given in Figure 8. Figure 9 shows the computed transmission data of this DSL element FSS for the incident angle steered from normal to 45° . The resonant frequencies are very stable with respect to the incident angle variation and are near the design frequencies, i.e. 8.45 GHz and 33 GHz. Figure 10 shows representatively the good agreement between the measured and computed results at normal incidence. This verified the 4-frequency integrated design based on the IEF approach. Table 1 summarizes the computed RF loss performance of this DSL element FSS. Note that the losses at 2.3 and 13.8 GHz are the transmission losses **while** the losses at other **frequencies** are reflection losses.

The single screen FSS has the advantages of lower mass, smaller volume, and easier fabrication than the double screen approach, **since neither accurate alignment** nor a dielectric spacer with uniform thickness and dielectric properties is required. However, to insure that the multi-band FSS operates at all the bands, high dielectric constant substrate is required for eliminating the grating lobe at the high frequencies. Currently, none of the high dielectric constant materials (e.g., the Duroid 6010.5 laminate) has been qualified for space applications. Therefore, the following double screen DSL element FSS is considered for the Cassini 4-frequency FSS.

V. Double Screen 4-Frequency FSS

As mentioned in Section I, one can add a low-pass (or **Ka-add-on**) FSS in front of the **tri-band** FSS to form the **Cassini** double screen 4-frequency FSS. In operation, the **Ka-** and **X-band** waves are reflected by the front (top) and back (bottom) grids, respectively. Both **S-** and **Ku-band** waves will pass through this dual-screen FSS with minimum RF insertion loss. The 3-frequency FSS has been described in Section III. Hence in this section the design and performance of a single screen **Ka-add-on** FSS will be discussed first, then the cascading of the **Ka-add-on** and 3-frequency FSSs (or the double screen 4-frequency FSS) will be described next.

Figure 11 shows a single thin screen **Ka-add-on** FSS etched on a 1 mil thick and 20" by 20" sized Kapton substrate. Figure 12 shows representatively the good agreement between the measured and the calculated transmission results at normal incidence. It also shows that this **Ka-add-on** FSS is designed to reflect the **Ka-band** wave and to transmit the lower frequency waves at **S-**, **X-**, and **Ku-band**. Thus it is also called a low-pass FSS. Similarly the **Ka-add-on** FSS may be designed with the presence of a Kevlar honeycomb, as shown in Figure 13. The predicted transmission performance is plotted in Figure 14 for the incident angle steered from normal to 45° and for both **TE** and **TM** polarizations. Figure

15 illustrates the comparison between the computed and measured data for this FSS'S transmission performance. Again good agreement between the measured and calculated results via the IEF approach is observed.

The cascading of two non-similar FSS screens is very difficult to analyze exactly. However, using the following systematic procedures, a single-mode cascading approach may readily be employed to get a first order assessment of this double-screen FSS'S performance. Consider the double-screen FSS as shown in Figure 2b. First, one divides the FSS at the mid-plane of the Kevlar honeycomb. Upwards from this middle plane is considered the first FSS screen section, and below this plane is the second FSS screen section. Each FSS section can be accurately modelled by the single screen FSS analysis described earlier. Since the dividing plane is electrically far from the FSS grid and the FSS element spacing is less than a half wavelength, one can assume that only the 0th order mode is significant, Thus one may next cascade the two sections by converting the scattering matrix [s] from each section to a transmission matrix [t] and multiplying the resulting [t] matrices. The conversion from [s] matrix to [t] matrix is the same as that described in [18,19]. The final [t] matrix product is then converted back to a scattering matrix, which yields the transmission and reflection coefficients for the double screen FSS.

The Ka-add-on FSS (Figure 11) and the 3-frequency FSS (Figure 3) were assembled together with a foam spacer and evaluated as a 4-frequency FSS. The foam spacer is a 0.75" thick Rohacell 51-IG foam. The good agreement between the predicted and measured transmission performances of this double screen FSS is shown in Figure 16 for normal incidence, representatively. This verified the accuracy of this efficient method and the add-on 4-frequency FSS design approach. The computed loss performance at the four bands (i.e. S/X/KU/KA bands) is summarized in Table 2. Note that the losses at 2.3 and 13.8 GHz are the transmission losses while the losses at 7.2, 8.4, 32 and 34 GHz are reflection losses,

Next the **Ka-add-on** and the 3-frequency FSSS were bonded on the top and bottom sides of a **Kevlar** honeycomb as shown in Figure 2. A representative comparison between the measured and computed transmission performances of this double screen FSS is shown in Figure 17 with normal incidence. Note that there is no S band measured data, since the measurement requires much larger size than the present 20" by 20" at this particular frequency. Nevertheless, the accuracy of the **DSL** element FSS design software has been checked thoroughly by measurements at higher frequencies. Thus the computed results at S-band are considered to be accurate. The computed **RF loss performance** for this double screen FSS is summarized in Table 3. The losses are higher than the two screen FSS's losses without the **Kevlar** honeycomb as indicated in Table 2. This is due to the relatively higher loss tangent of the **Kevlar/Epoxy** skin materials.

VI. Conclusion

Analysis, design and test results are presented for multi-band FSSS with DSL patch elements. Good agreement between the measured and computed results verifies the various design approaches described in this paper. For applications in the NASA Cassini Project, the single screen DSL element FSS has been successfully demonstrated for both a **tri-** and **4-band** FSS. In another parallel effort using the double **ring FSS** elements [8], it was found that only the **tri-band** application can be designed with the single screen approach. This implies that the DSL element is superior to the double ring element for multi-band (≥ 4 -band) FSS applications. Because the **Duroid 6010.5** substrate has not yet been qualified for space applications, the double screen DSL FSS with a **Kevlar** honeycomb was also developed for the **Cassini 4-frequency FSS**.

Acknowledgement

The work described in this article was carried out by the Jet Propulsion Laboratory, California Institute of Technology, under contract with the National Aeronautics and Space

Administration. The author wishes to thank Dr. J. **Vacchione** for providing the double screen FSS results of Figure 16, Dr. Ken Woo for managerial support, Mr. G. Hicky for fabricating the honeycomb sandwiches, and Mr. Cosine Chavez for performing the FSS measurements.

References

1. G.I-I. Schennum, "Frequency-selective surfaces for multiple frequency antennas," Microwave Journal, vol. 16, pp. 55-57, May 1973.
2. V.D. Agrawal and W.A. Imbriale, "Design of a dichroic Cassegrain subreflector," IEEE Trans., vol. AP-27, no.4, pp. 466-473, July 1979.
3. K. Ueno, et al, "Characteristics of FSS for a multi-band communication satellite", 1991 Int. IEEE AP-S Symposium Digest, pp. 735-738, Ontario, Canada, June 1991.
4. T. K. Wu, "Single screen triband FSS with double-square-loop elements," Microwave and Optical Tech. Letters, vol.5, no.2, pp. 56-59, Feb. 1992.
5. T. K. Wu, "Double-square-loop FSS for multiplexing four (S/X/Ku/Ka) bands", 1991 Int. IEEE AP-S Symposium Digest, pp. 1885-1888, Ontario, Canada, June 1991.
6. J. Huang and S.W. Lee, "Tri-band FSS with circular ring elements," 1991 Int. IEEE AP-S Symposium Digest, pp. 204-207, Ontario, Canada, June 1991.
7. T.K. Wu, et al, "Multi-ring element FSS for multi-band applications," 1992 Int. IEEE AP-S Symposium Digest, pp. 1775-1778, Chicago, IL, July 1992.
8. T.K. Wu, M. Zimmerman and S.W. Lee, "Evaluation of frequency selective reflector antenna systems," Microwave and Optical Technology Letter- vol.6, n0.3, pp. 175-179, March 1993.
9. P. Callaghan, E. Parker, and R. Langley, "Influence of supporting dielectric layers on the transmission properties of frequency selective surfaces," IEE Proceeding-H, vol. 138, no.5, pp. 448-454, Oct. 1991.

10. R.J. Langley and E.A. Parker, "Double-square frequency-selective surfaces and their equivalent circuit," Electronics Letters, vol.19, no.17, p.675, Aug. 18, 1983.
11. C. K. Lee and R. Langley, "Equivalent circuit models for frequency selective surfaces at oblique angle of incidence," IEE Proceedings, vol.132, pt. H, no. 6, pp.395-398, Oct. 1985.
12. I. Anderson, "On the theory of self-resonant grids," Bell System Tech. J., vol.54, pp. 1725-1731, Dec.1975.
13. T. K. Wu, "Quasi-optical grids with rectangular patch/aperture elements," Int. J. of Infrared and MMW, vol. 14, no. 5, pp. 1017-1033, May, 1993.
14. R. Mittra, C. Chan and T. Cwik, "Techniques for Analyzing Frequency Selective Surfaces - a Review," IEEE Proceedings, vol. 76, no, 23, Dec. 1988, pp. 1593-1615.
15. B. J. Rubin and H. L. Bertoni, "Reflection from a periodically perforated plane using a subsectional current approximation," IEEE Trans., AP-31, no. 6, pp. 829-836, "Nov. 1983.
16. S.W. Lee, "Scattering by Dielectric-Loaded Screen," IEEE Trans., vol. AP-19, no. 5, p.656, Sept. 1971.
17. C.C. Chen, "Diffraction of electromagnetic waves by a conducting screen perforated with circular holes," IEEE Trans. vol. MTT-19, pp. 475-481, May 1971.
18. J. Vacchione and T.K. Wu, "Analysis of a dual, non-similar, screen FSS using simple cascading procedures," 1992 Int. IEEE AP-S Symposium Digest, pp. 1779-1782, Chicago, Illinois, July 1992. "
19. S. Ramo, et. al., Fields and Waves in Communication Electronics, John Wiley & Sons, Inc., N. Y., p. 605, 1965.

Figure Captions

1. Proposed **Cassini** high gain antenna with a 4-frequency FSS.
2. **Cassini** 4-frequency FSS design approaches.
3. Configuration of the thin screen **tri-band** FSS.
4. Computed transmission performance of the thin screen **tri-band** FSS.
5. Transmission characteristics of the thin **screen tri-band** FSS at 15° TM incidence.
6. Configuration of the single screen **tri-band** FSS with a **Kevlar** Honeycomb.
7. Comparison of computed and measured transmission performance of the **tri-band** FSS with the **Kevlar** honeycomb.
8. Configuration of the single screen 4-frequency FSS with a **Kevlar** honeycomb.
9. Computed transmission characteristics of the single screen 4-frequency FSS with the **Kevlar** honeycomb.
10. Comparison of computed and measured transmission performance of the single screen 4-frequency FSS with the **Kevlar** honeycomb at normal incidence.
11. Configuration of the thin screen **Ka-add-on** FSS.
12. Comparison of the computed and measured transmission characteristics of the thin screen **Ka-add-on** FSS at normal incidence.
13. Configuration' of the single screen **Ka-add-on** FSS with a **Kevlar** honeycomb.
14. Computed transmission performance of the **Ka-add-on** FSS with the **Kevlar** honeycomb,
15. Comparison of computed and measured transmission performance of the single screen **Ka-add-on** FSS with the **Kevlar** honeycomb at normal incidence.
16. Comparison of computed and measured transmission performance of the double **screen** 4-frequency FSS without the **Kevlar** honeycomb.
17. Comparison of computed and measured transmission performance of the double screen 4-frequency FSS with the **Kevlar** honeycomb.

Table 1. Computed Loss (dB) of the Single Screen 4-Frequency FSS

Frequency GHz	$\Theta_i = 0^\circ$	30°		45°	
		TE	TM	TE	T M
2.3	.95	1.2	.73	1.6	.5
7.2	.45	.37	.61	.27	.9
8.4	.08	.07	.11	.06	.16
13.8	.37	.56	.29	.9	.2
32	.09	.17	.13	.16	.69
34	.14	.2	.21	.13	.43

Table 2. Computed Loss (dB) of the Double Screen 4-Frequency FSS no Honeycomb

Frequency GHz	$\Theta_i = 0^\circ$	30°		40°	
		TE	TM	TE	TM
2.3	.42	.48	.33	.55	.28
7.2	.24	.28	.44	.33	.73
8.4	.04	.01	.01	.02	.03
13.8	.46	.23	.17	.23	.15
32	.33	.2	.3	.06	.27
34	.02	.04	.03	.17	.18

Table 3. Computed **Loss** (dB) of the Double Screen 4-Frequency FSS with Honeycomb

Frequency GHz	$\Theta_i = 0^\circ$	30°		45°	
		TE	TM	TE	TM
2.3	.41	.5	.33	.68	.23
7.2	.65	.73	1.1	.85	1.95
8.4	.14	.17	.19	.22	.29
13.8	1.1	1.2	.73	2.1	.53
32	.53	.19	.22	.21	.48
34	.21	.28	.33	.2	.3

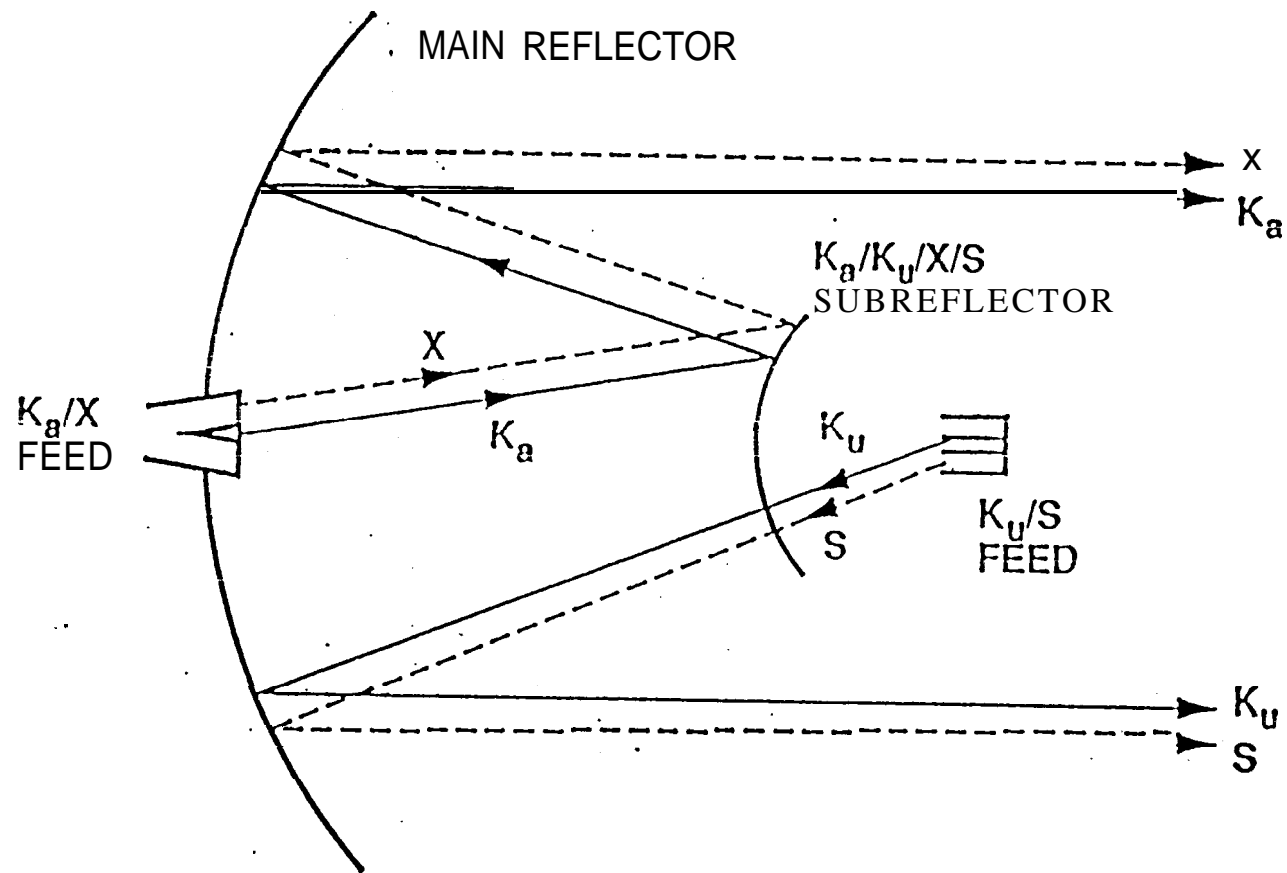
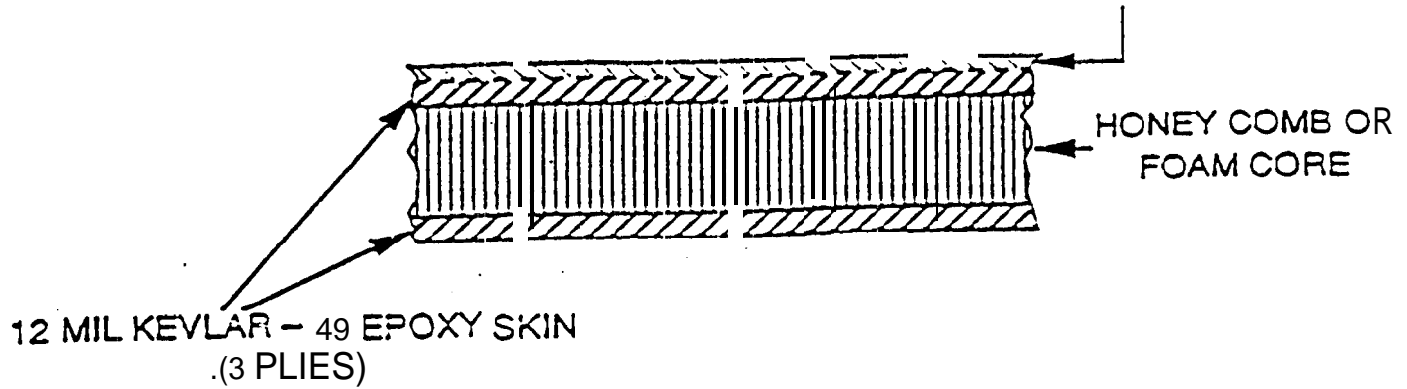


Fig. 1

(a)

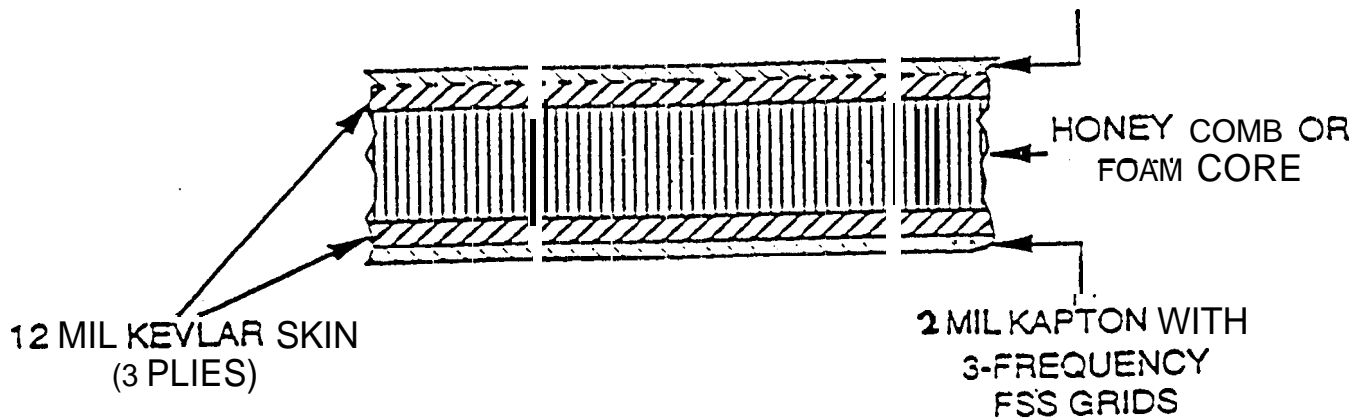
10 MIL DUROID 6010.5 (WITH FSS GRIDS)



SINGLE SCREEN DESIGN

(b)

2 MIL KAPTON WITH Ka-ADD-ON FSS GRIDS



DOUBLE SCREEN DESIGN

Fig. 2

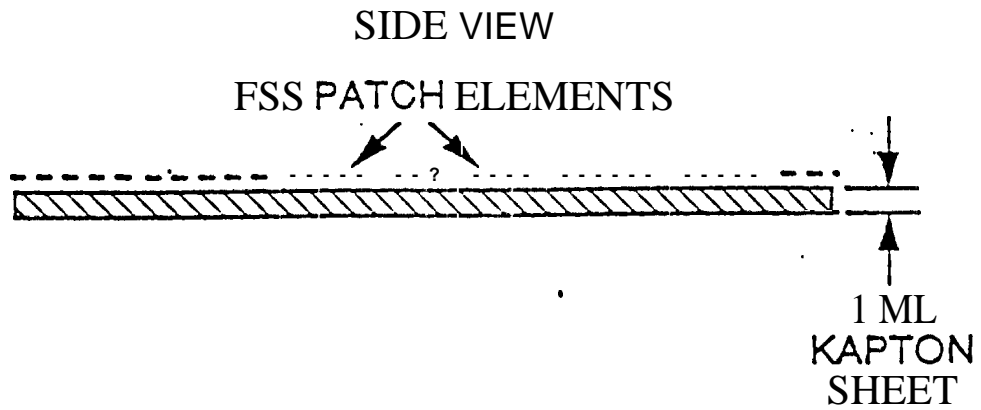
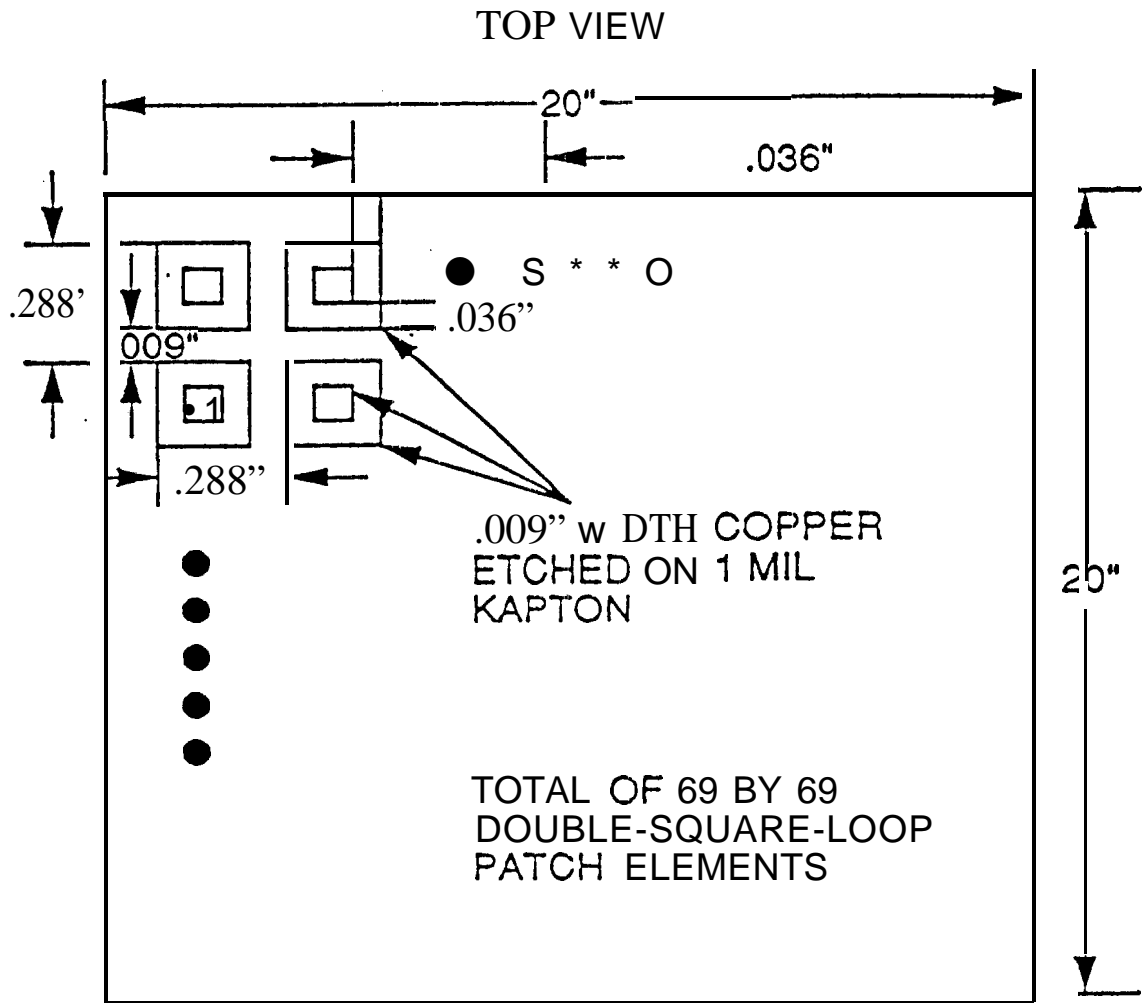


Fig. 3

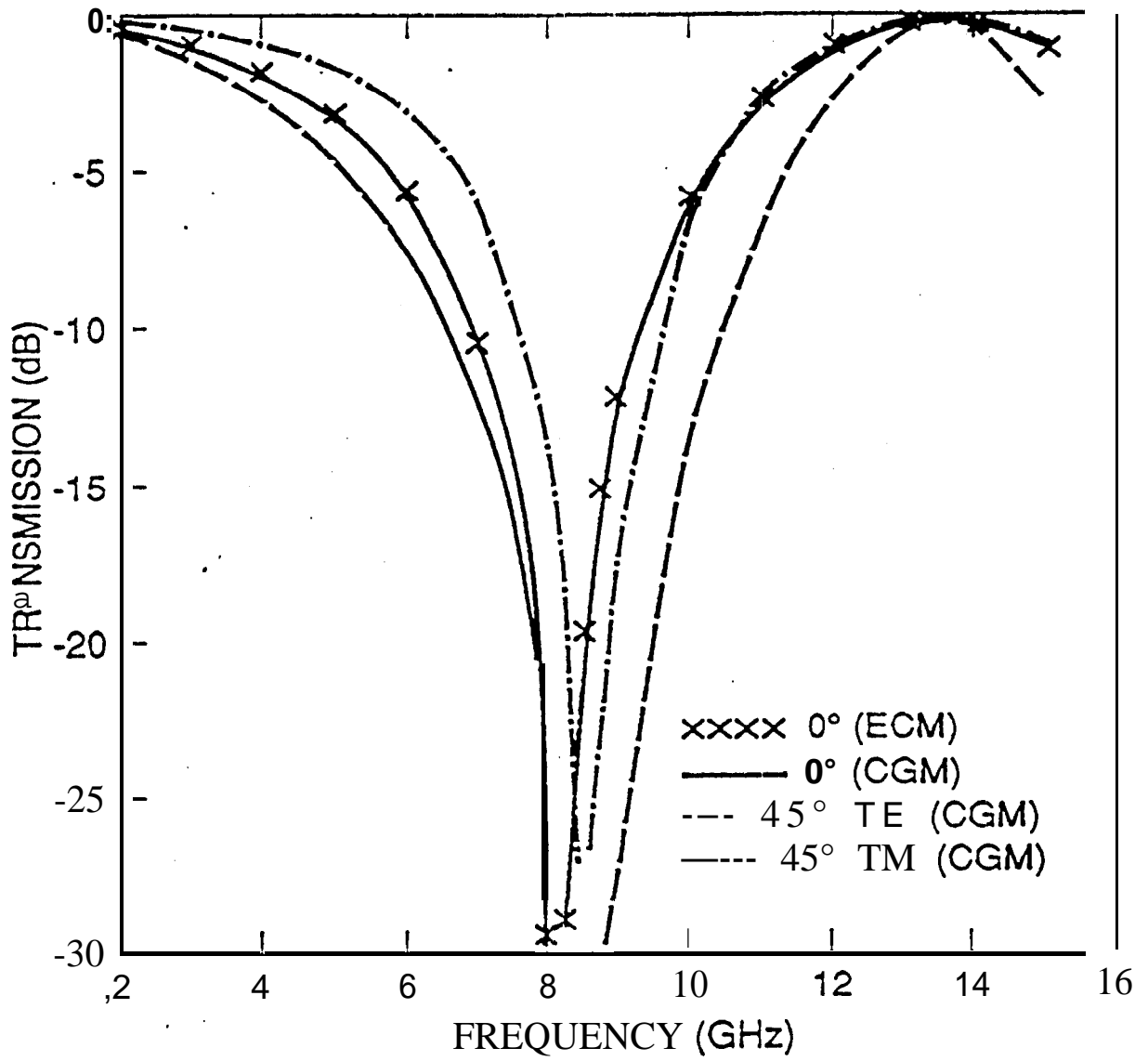


Fig. 4

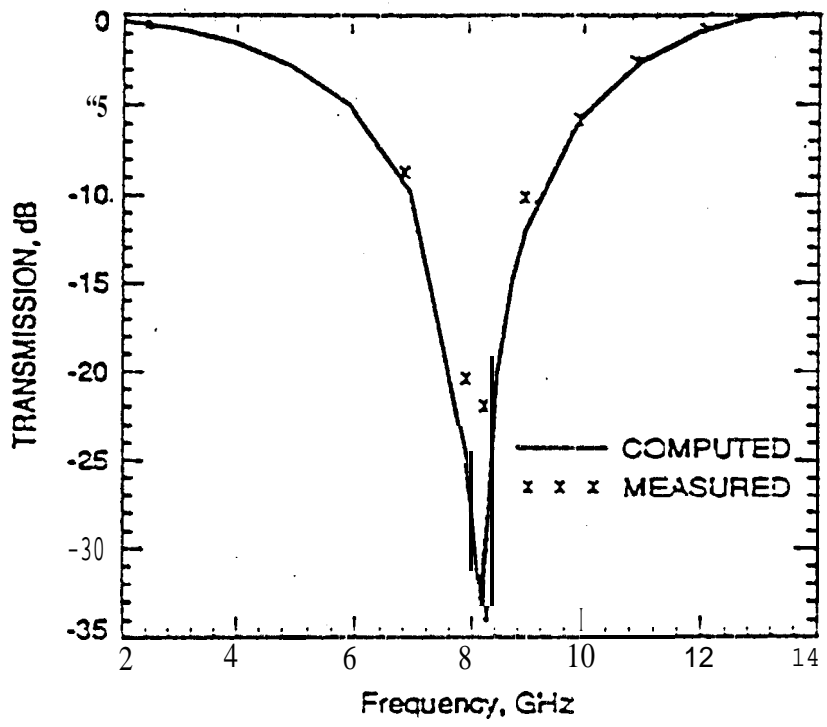


Fig. 5

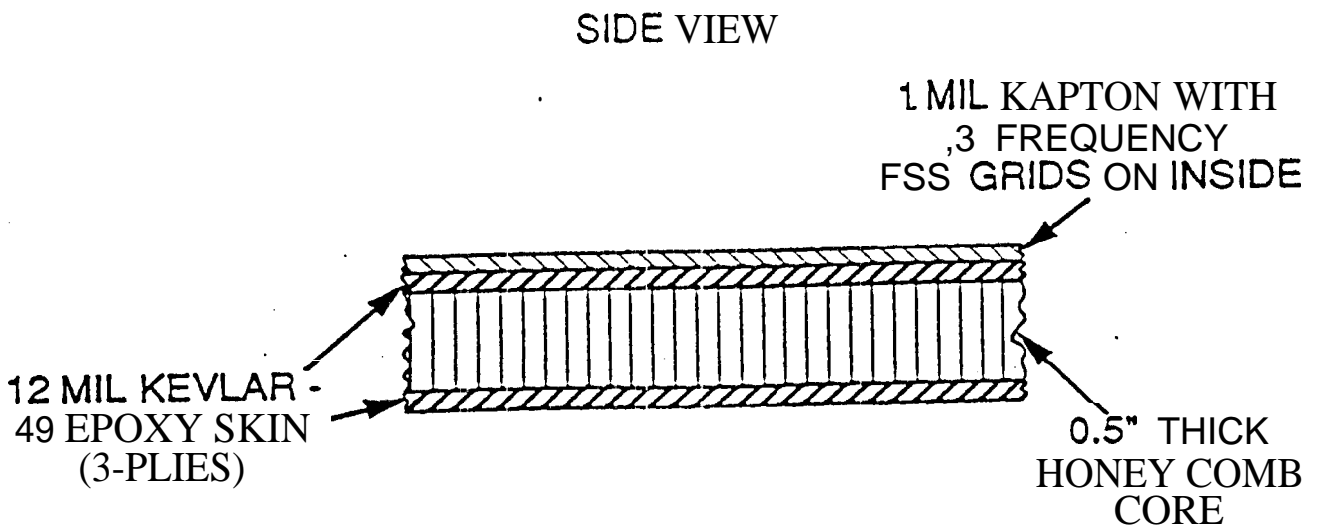
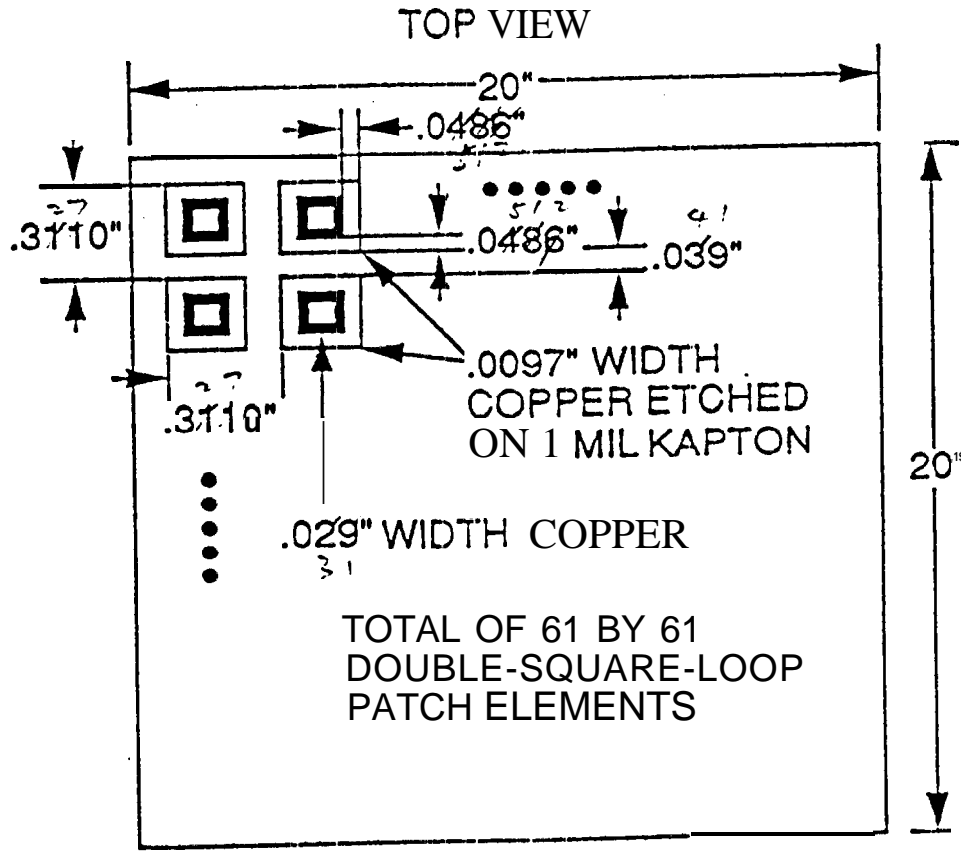
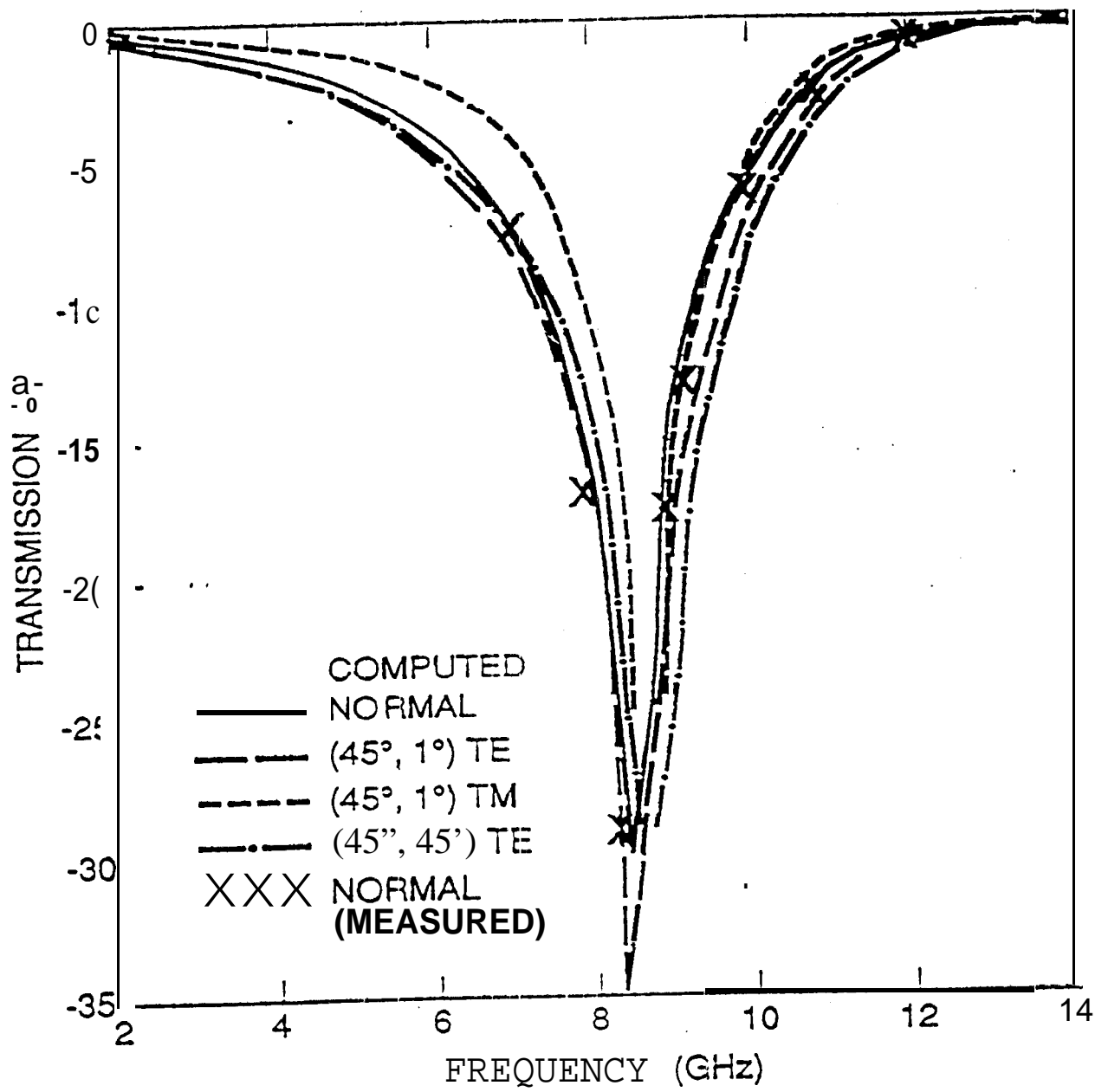


Fig. 6



1-2-7

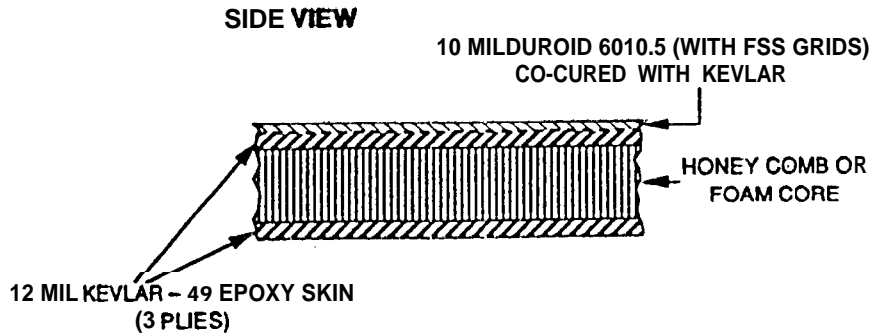
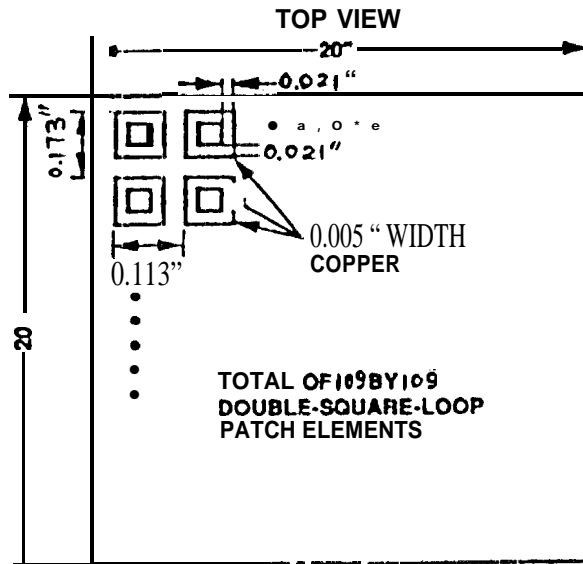


Fig. 8

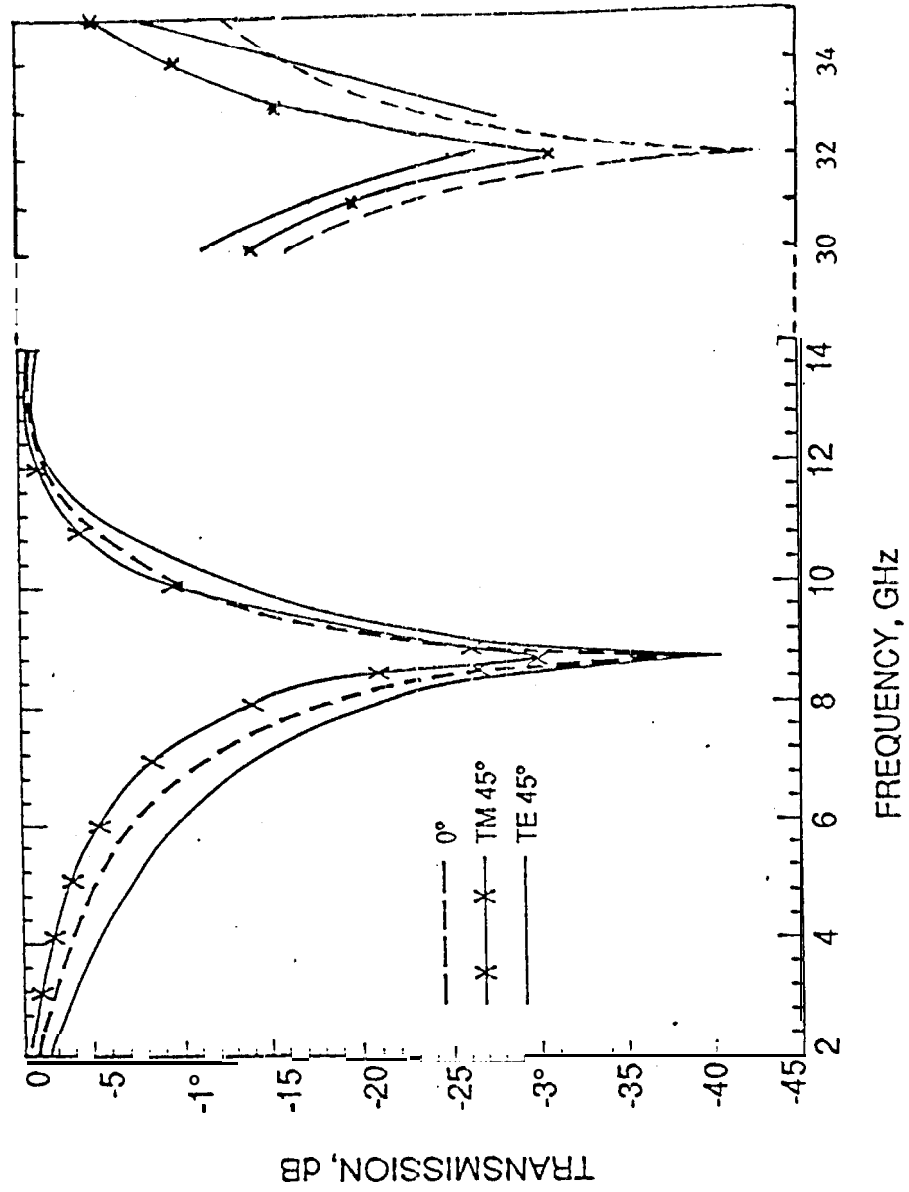


Fig. 9

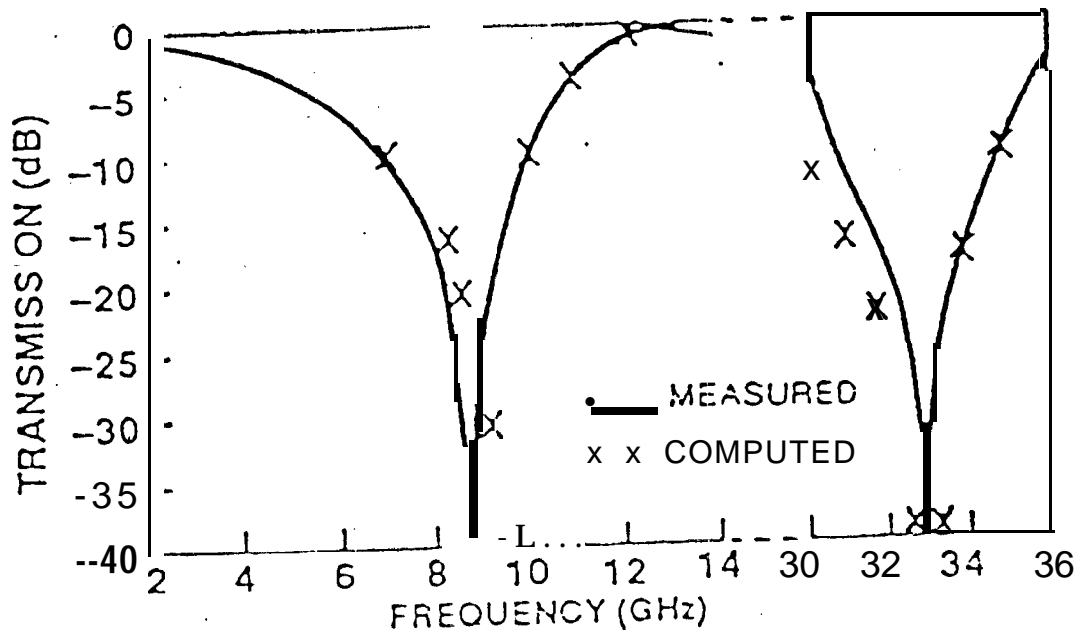
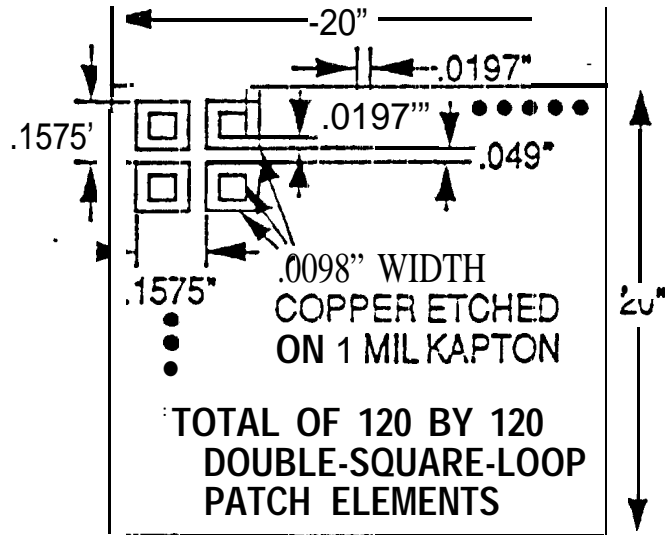


Fig. 10

TOP VIEW



SIDE VIEW

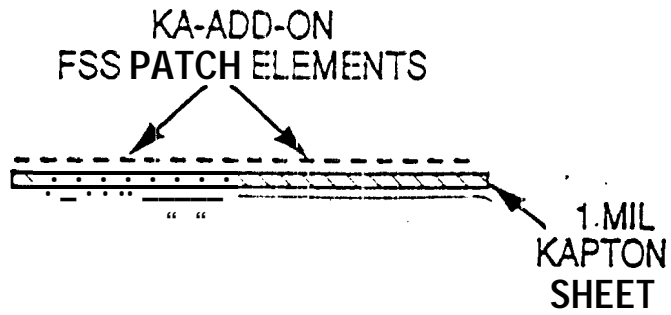
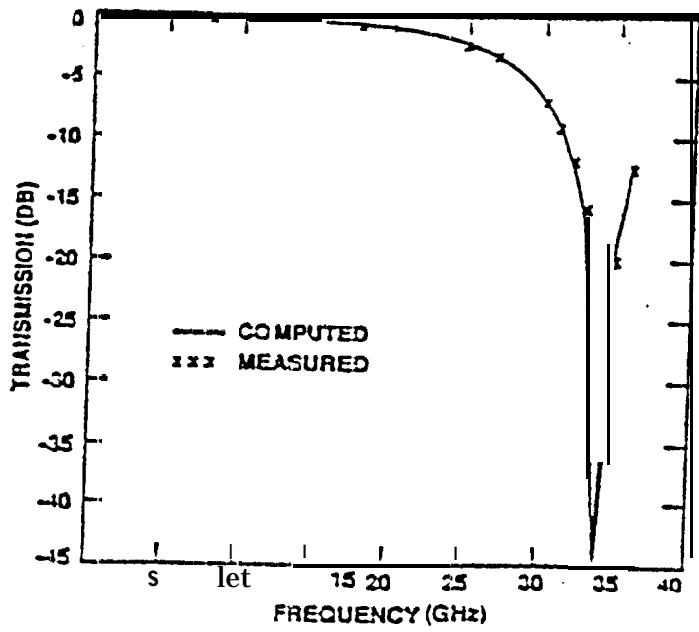


Fig. 11



Figure

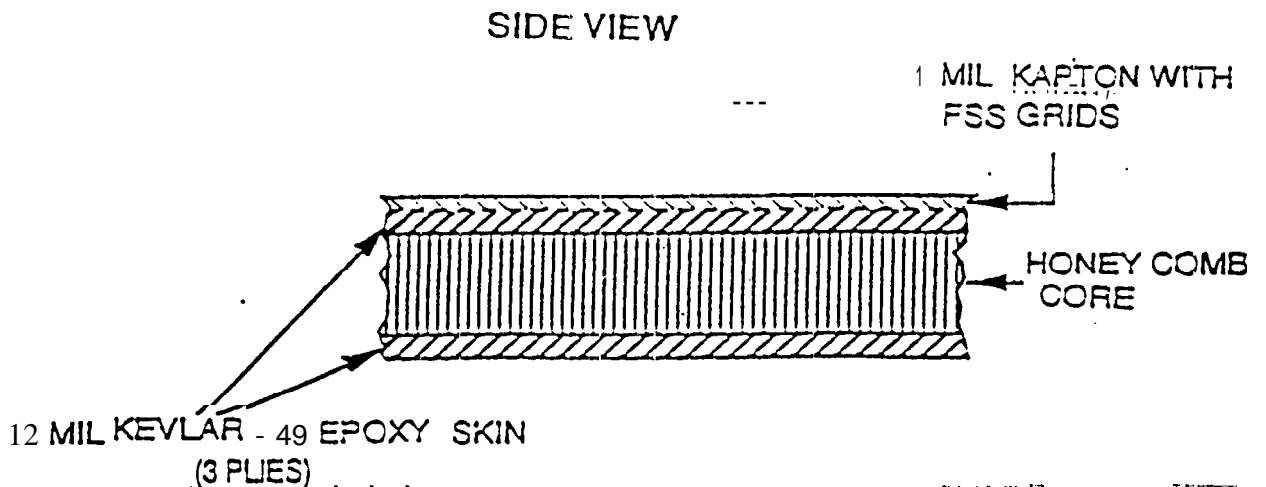
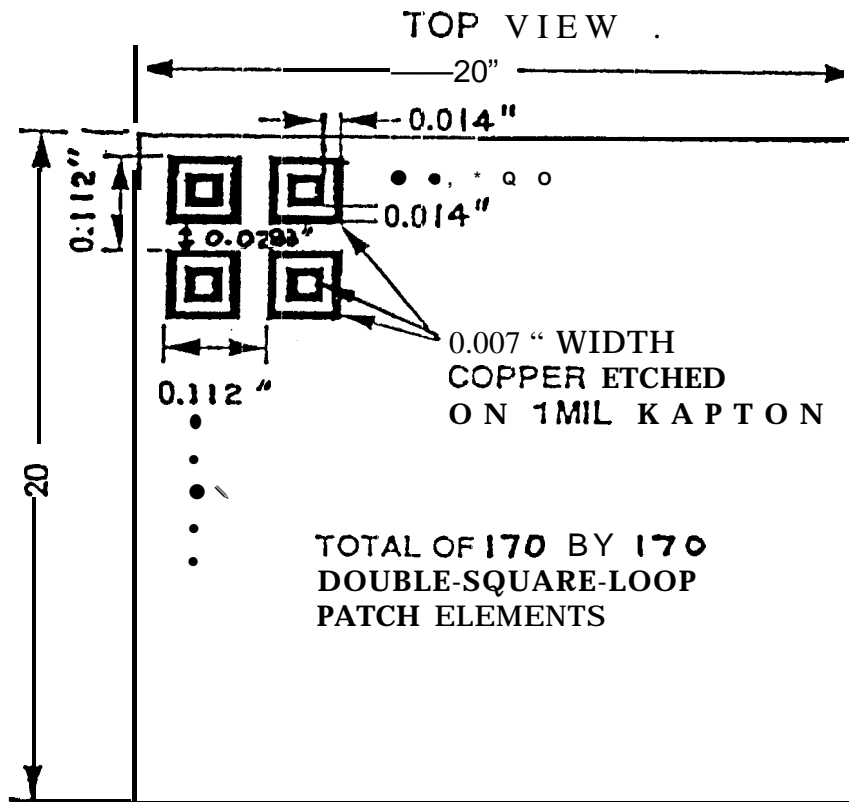
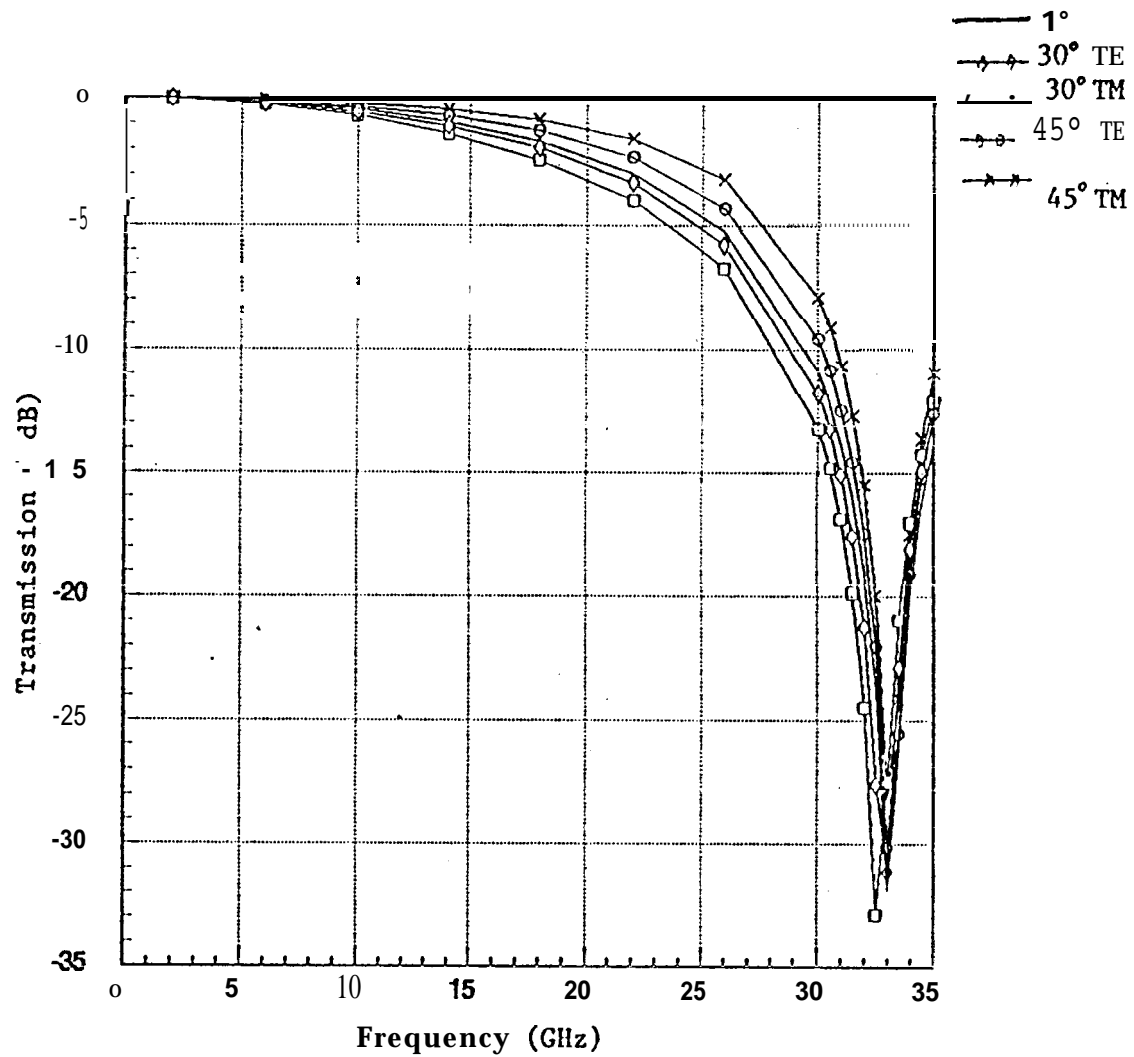


Fig. 13

Fig. 14



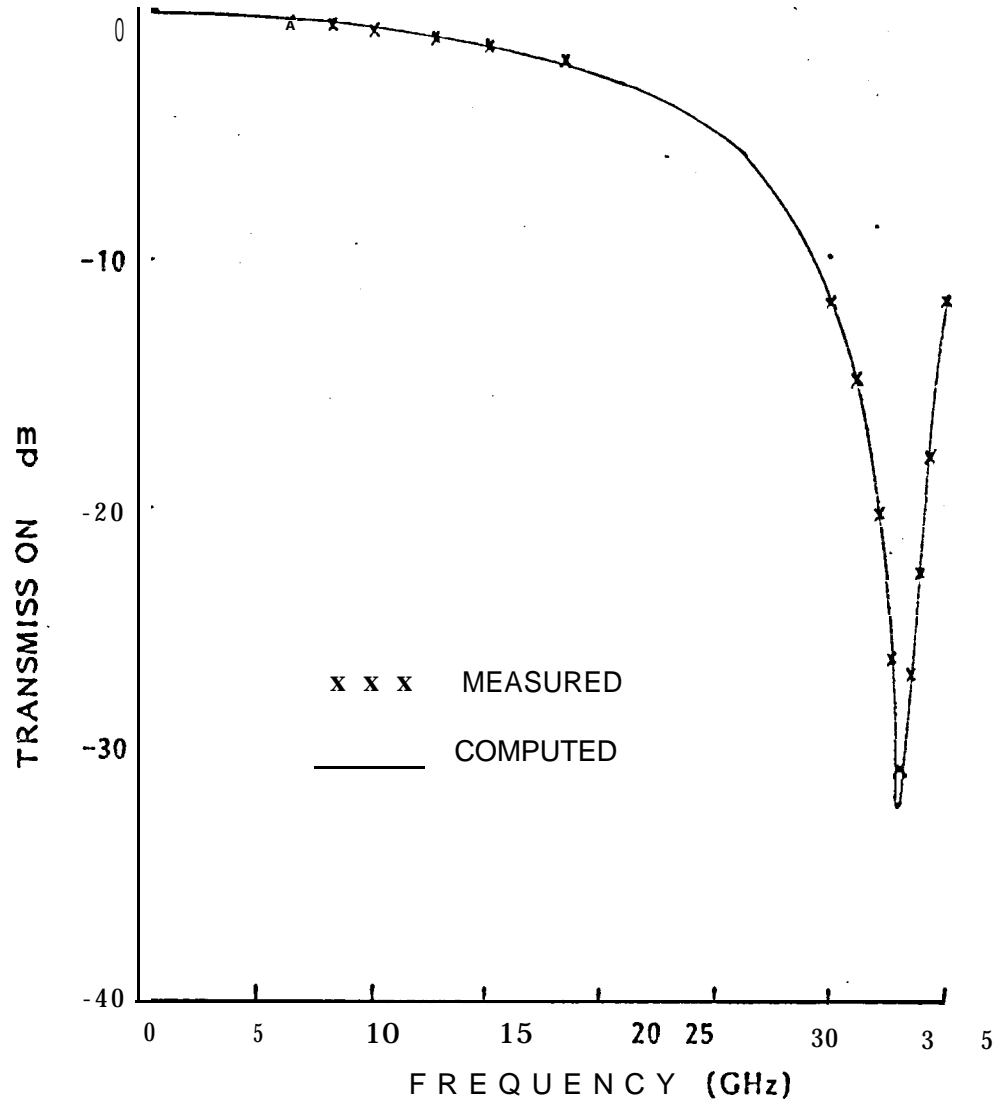


Fig. 1x-

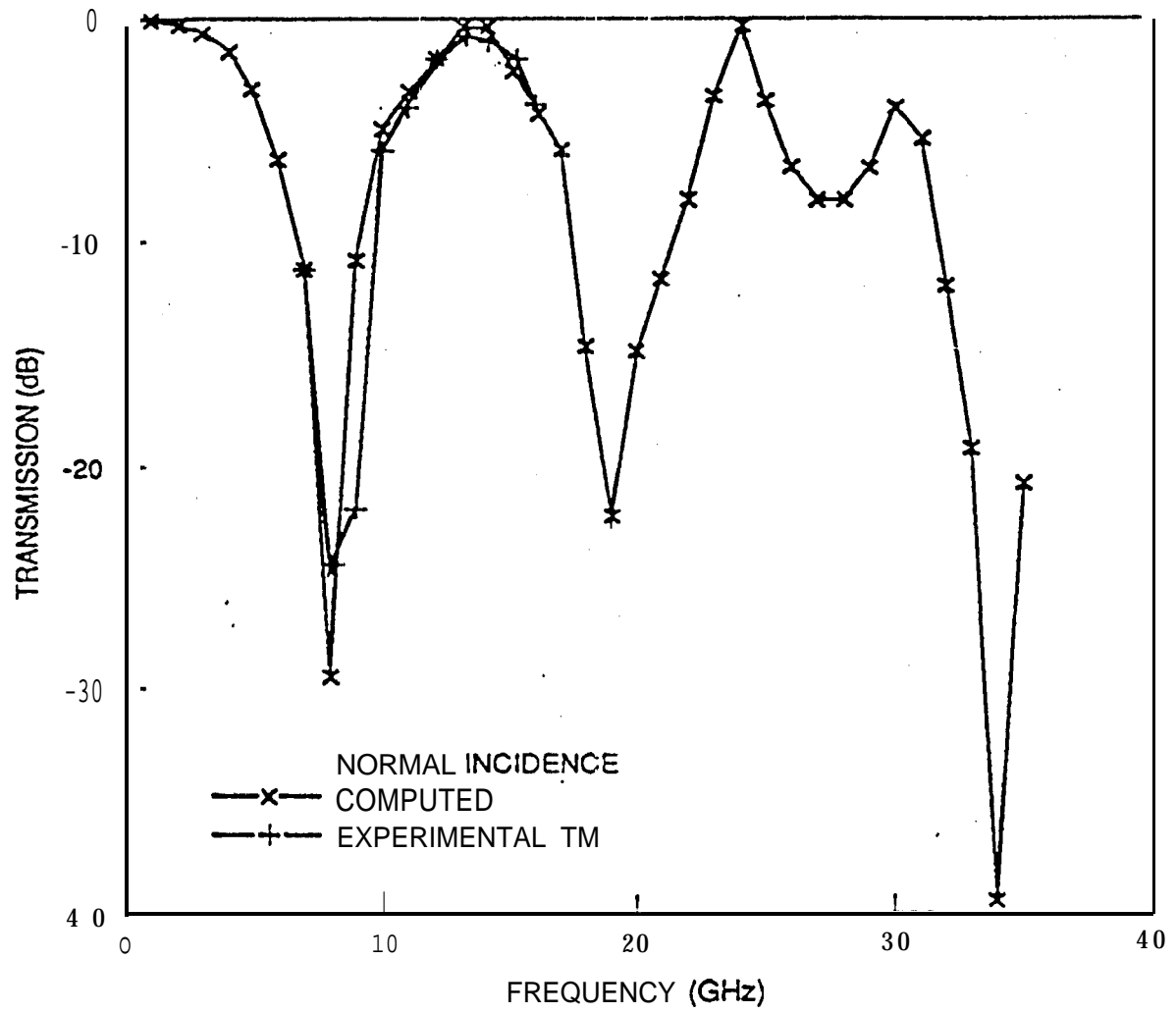


Fig. 16

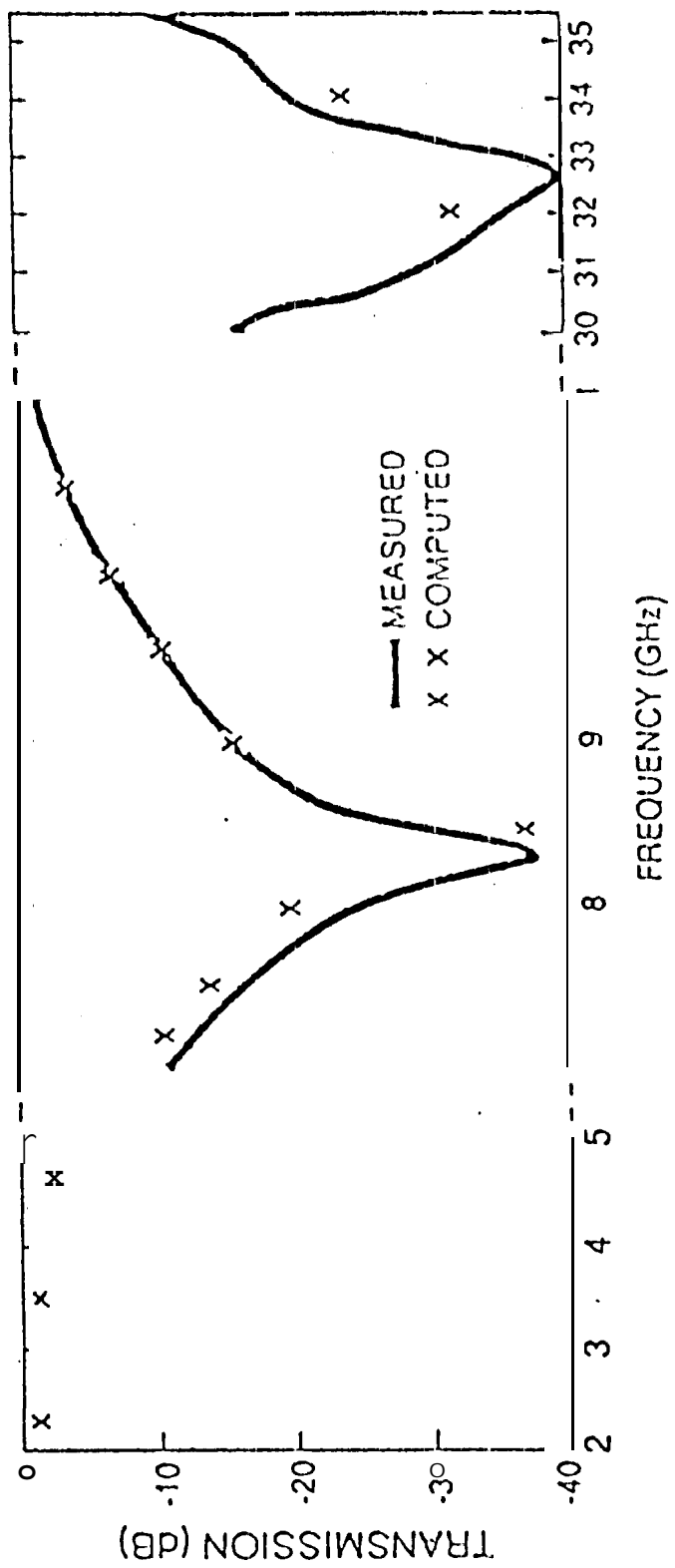


Fig. 17